Fermi-Liquid Theory of a Quantum Dot

Sören Arlt

München 2016

Fermi-Flüssigkeits-Theorie eines Quanten Punktes

Sören Arlt

Bachelorarbeit
an der Fakultät für Physik
der Ludwig–Maximilians–Universität
München

vorgelegt von
Sören Arlt
aus Großenhain

München, den 4. Juli 2016

Gutachter: Professor Jan von Delft
Tag der mündlichen Prüfung: 6. Juli 2016

Contents

Chapter 1

Introduction

Quantum dots (QDs) are systems that confine an electron to the range of its de Broglie wavelength in all three dimensions [1]. As electronic devices like resistors and transistors become smaller, new properties arise from quantum mechanics. The study of QDs could provide important insight on the transport properties of small electronic devices [2].

QDs are also of great interest for the construction of quantum gates and quantum bits for quantum information processing [3][4]. A QD with tunable properties can easily be realized experimentally (Fig. 1.1). Theoretical results thus have a good chance to be examined in experiment.
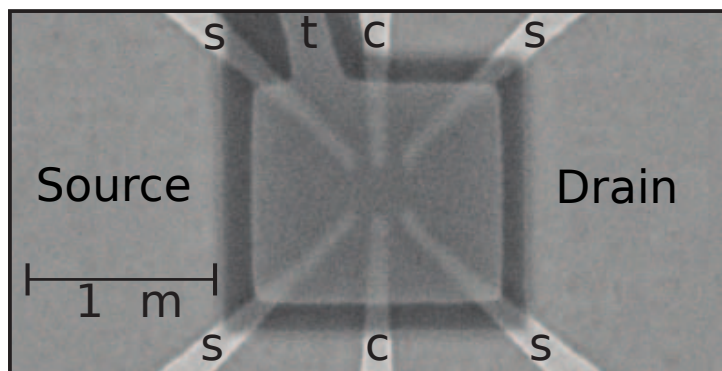

Figure 1.1: Experimental realization of a quantum dot: Electrons are constrained to two dimensions 85 nm beneath the surface of a GaAs/AlGaAs heterostructure. The potential structure between a source and a drain contact can be tuned by applying voltage to the central- and side gates **c** and **s**. Increasing the voltage at the top gate **t** increases the carrier density of the two-dimensional electron system in the central constricted region and hence the chemical potential. If we limit the applied voltages to be negative, the propagation between the two contacts is confined to a narrow channel and the system can be described by a single dimension. If the side gate voltage is higher than the central gate voltage, discrete levels form in the central region. Figure 1a in [5].

In this thesis, we want to examine the properties of a QD in one dimension. We will see that the levels in a QD can effectively be modelled by the Single Impurity Anderson Model (SIAM), which was introduced by Anderson in 1961 to describe localized magnetic states in metals [6]. The SIAM consists of a single level with interaction and couples to leads on both sides. Despite its simple construction, the SIAM is highly nontrivial and offers a lot of interesting behavior. The Kondo model, which explains an anomalous resistivity minimum in dilute magnetic alloys, can be acquired as a limit of the SIAM, where a single magnetic state forms.

Nozières formulated a Fermi-liquid theory of the Kondo model, describing its low-temperature behavior in terms of weakly interaction quasiparticles [7]. This approach was generalized to the SIAM in Ref. [8].

We will explore how this Fermi-liquid theory can be applied to the QD. We calculate scattering phases and susceptibilities numerically using a program by Lukas Weidinger based on the functional renormalization group (fRG). The fRG program produces data for zero temperature and at equilibrium. Once we find the FL parameters of the QD, we can compute transport coefficients and are able to describe conduction behavior at low magnetic fields, temperatures and bias voltages.

We follow two approaches. For approach (A), we appoint an effective SIAM level position to QDs of varying gate voltage. We improved on a previous calculation of the Fermi-liquid parameters by Phillip Rosenberger [9]. Since the QD is significantly more complicated than the SIAM, this model will not be perfectly accurate. We will see where and how the SIAM description fails.

We can also attempt to describe the QD in terms of Fermi-liquid theory without assigning an effective level by varying the chemical potential. We will show advantages and disadvantages of this approach and compare both results.

Showing that approaches (A) and (B) yield equivalent results for the transport coefficients, we gain important understanding for systems that cannot be assigned an effective level position.

Chapter 2

SIAM and Fermi-liquid Theory

2.1 SIAM

The Single Impurity Anderson Model (SIAM) describes a level of energy ϵ_d occupied by particles with spin up or down, with number operators $n_{d,\uparrow}$ and $n_{d,\downarrow}$. The Hamiltonian is

$$H_d = \sum_\sigma \epsilon_d n_{d,\sigma} + U n_{d,\uparrow} n_{d,\downarrow}, \tag{2.1}$$

summing over spins σ. The number operators can be expressed by creation- and annihilation operators in the impurity: $n_{d,\sigma} = c_{d,\sigma}^\dagger c_{d,\sigma}$. The impurity couples to leads on both sides (L/R). The kinetic energy $\epsilon_{k\sigma}$ of particles with momentum k in the leads is

$$H_{L/R} = \sum_{k,\sigma} \epsilon_{k\sigma} n_{L/R,k\sigma}. \tag{2.2}$$

Again, the number operators are a combination of creation- and annihilation operators: $n_{L/R,k\sigma} = c_{L/R,k\sigma}^\dagger c_{L/R,k\sigma}$ The hopping from each one of the leads to the impurity and vice versa is expressed by additional terms of the Hamiltonian.

$$H_{\text{hop}} = \sum_{k,\sigma} \tau (c_{L,k\sigma}^\dagger c_{d,\sigma} + c_{R,k\sigma}^\dagger c_{d,\sigma} + h.c.). \tag{2.3}$$

τ is the hopping energy. The full Hamiltonian is the sum of these terms

$$H_{\text{SIAM}} = H_L + H_R + H_{\text{hop}} + H_d. \tag{2.4}$$

In the next section we want to show an approach to find the low-energy conductance behavior of the SIAM by generalization of Nozières Fermi-liquid Theory.

2.2 Scattering and Fermi-liquid Theory

Properties such as the conductance behavior as a function of magnetic field, temperature and bias voltage at low energies can be extracted from considering an effective Fermi-liquid theory [8], i.e. weakly interacting quasiparticles representing the behavior of the system. In this section we want to introduce the required scattering theory along with the essential Landauer-Büttiker formula and the Friedel sum rule.

2.2.1 Scattering

Lead electrons

We want to describe the conductance of the electrons in a metal with impurities. We do this by describing their scattering off an impurity. The electron states before and after scattering can be described by eigenstates of the free Hamiltonian $H_{L/R}$ [10].
The behavior in the leads is modelled by tight binding chains. Position is described by discrete sites and hopping between nearest neighbors is possible. In many solid state physics applications these sites correspond to single atoms. Here, the lattice is artificial. The spacing between the lattice sites is much larger than the spacing of the underlying crystal. We can write the Hamiltonian of each one of the (half-infinite) leads in second quantization with a hopping energy τ between nearest neighbors i and j:

$$H_{\text{hop}} = \sum_{\langle i,j \rangle}^{\infty} \sum_{\sigma} \tau(c_{j,\sigma}^{\dagger} c_{i,\sigma} + c_{i,\sigma}^{\dagger} c_{j,\sigma}). \tag{2.5}$$

The eigenstates of this Hamiltonian are found to be

$$|\psi_{k,\sigma}\rangle = \sqrt{\frac{2C}{\pi}} \sum_{j=1}^{\infty} \sin(kj) |j, \sigma\rangle, \tag{2.6}$$

for $k \in \left(0, \frac{\pi}{C}\right)$, where C is the lattice spacing [11]. By considering the eigenvalues

$$H_{\text{hop}} |\psi_{k,\sigma}\rangle = \omega(k) |\psi_{k,\sigma}\rangle, \tag{2.7}$$

we find the dispersion relation to be

$$\omega(k) = 2\tau \cos k. \tag{2.8}$$

For the scattering at the impurity we will need the local density of states of the lead electrons at the contact point, i.e. the end point of the half infinite chain. This is given by components of the retarded Green's function $G^{\sigma,R}$ [11]:

$$\rho_c^{\sigma}(\omega) = -\frac{1}{\pi} \text{Im}(G_{11}^{\sigma,R}). \tag{2.9}$$

The retarded Green's function of a system with Hamiltonian H and frequency ω is

$$G^R = \frac{1}{\omega - H + i0^+}. \tag{2.10}$$

To calculate the G_{11} component of the Green's function we follow the calculation of [12]. Another site is added at the end of the tight-binding chain. The hopping between the aditional site and the next is considered a perturbation V. g is the unperturbed Green's function.

$$
G = \begin{pmatrix} G_{11} & G_{12} & G_{13} & \cdots \\ G_{21} & G_{22} & G_{23} & \cdots \\ G_{31} & G_{32} & G_{33} & \cdots \\ \vdots & \vdots & \vdots & \ddots \end{pmatrix},
\tag{2.11a}
$$

$$
g = \begin{pmatrix} g_{11} & 0 & 0 & \cdots \\ 0 & G_{11} & G_{12} & \cdots \\ 0 & G_{21} & G_{22} & \cdots \\ \vdots & \vdots & \vdots & \ddots \end{pmatrix},
\tag{2.11b}
$$

$$
V = \begin{pmatrix} 0 & \tau & 0 & \cdots \\ \tau & 0 & 0 & \cdots \\ 0 & 0 & 0 & \cdots \\ \vdots & \vdots & \vdots & \ddots \end{pmatrix}.
\tag{2.11c}
$$

We write the Dyson equation

$$
G = g + gVG,
\tag{2.12}
$$

yielding the system of equations

$$
G_{11} = g_{11} + (gVG)_{11} = g_{11} + g_{11}V_{12}G_{21},
\tag{2.13}
$$
$$
G_{21} = g_{21} + (gVG)_{21} = g_{21} + g_{22}V_{21}G_{11}.
\tag{2.14}
$$

We obtain a quadratic equation in G_{11} by insertion:

$$
G_{11} = g_{11} + g_{11}\tau^2 G_{11}^2.
\tag{2.15}
$$

$g_{11} = [\omega - H_0]^{-1}$. With $H_0 = 0$, we can write $g_{11} = \frac{1}{\omega}$. Solving for G_{11}:

$$
G_{11} = \frac{\omega}{2\tau^2} \pm \frac{1}{2\tau^2}\sqrt{\omega^2 - 4\tau^2}.
\tag{2.16}
$$

We thus get our final expression for the density of states at the contact site,

$$
\rho_c^\sigma(\omega) = \frac{1}{2\pi\tau^2}\sqrt{4\tau^2 - \omega^2}.
\tag{2.17}
$$

Requiring the density to be a non-negative real number, the sign in Eq. (2.16) is fixed to $+$. It follows from Eq. (2.16) that $\rho^\sigma(|\omega| > 2\tau) = 0$, resulting in a total band width of 4τ.

S-matrix

The asymptotic states can be expressed in a basis of left lead eigenstates $\langle\psi_L|$ and right lead eigenstates $\langle\psi_R|$ by complex numbers. The S-matrix describes the evolution of an asymptotic state in the infinite past to asymptotic states in the infinite future.

$$\begin{pmatrix} C \\ D \end{pmatrix} = \lim_{t\to\infty, t'\to-\infty} \begin{pmatrix} \langle\psi_L|\,\hat{U}(t,t')\,|\psi_L\rangle & \langle\psi_L|\,\hat{U}(t,t')\,|\psi_R\rangle \\ \langle\psi_R|\,\hat{U}(t,t')\,|\psi_L\rangle & \langle\psi_R|\,\hat{U}(t,t')\,|\psi_R\rangle \end{pmatrix} \begin{pmatrix} A \\ B \end{pmatrix} = \begin{pmatrix} S_{LL} & S_{LR} \\ S_{RL} & S_{RR} \end{pmatrix} \begin{pmatrix} A \\ B \end{pmatrix} \quad (2.18)$$

We are interested in the phases the components of a complex vector pick up in the scattering process. The information about the impurity is brought into the S-matrix via the Green's function of the impurity $G^{\sigma,R}$. Considering impurities with multiple sites, such as the QD, we are interested in the S-matrix from their leftmost to their rightmost site l and r. As seen in [10] we can write the S-matrix as

$$S^\sigma = \mathbb{1} - 2\pi i\tau^2 \rho_c^\sigma(\omega=\mu) \begin{pmatrix} G_{l,l}^{\sigma,R} & G_{l,r}^{\sigma,R} \\ G_{r,l}^{\sigma,R} & G_{r,r}^{\sigma,R} \end{pmatrix}. \quad (2.19)$$

This utilizes the local density of states at the contact points ρ_0^σ, which we found earlier. The S-matrix is unitary ($S^\dagger = S^{-1}$). It is also symmetric ($S = S^\top$), if the impurity is symmetric (in particular $G_{l,r}^{\sigma,R} = G_{r,l}^{\sigma,R}$). We can diagonalize the S-matrix using $W = \frac{1}{\sqrt{2}}\begin{pmatrix} 1 & 1 \\ 1 & -1 \end{pmatrix}$:

$$W^\dagger S^\sigma W = \begin{pmatrix} e^{i\delta_{\sigma,s}} & 0 \\ 0 & e^{i\delta_{\sigma,a}} \end{pmatrix} = e^{i\delta_{ref}} \begin{pmatrix} e^{i2\delta_{\sigma,1}} & 0 \\ 0 & e^{i2\delta_{\sigma,2}} \end{pmatrix}. \quad (2.20)$$

δ_{ref} is a constant reference phase which will later be fixed at the same value for both spins. We define two more quantities:

$$\delta_{\sigma,+} = \delta_{\sigma,1} + \delta_{\sigma,2} = \frac{1}{2}(\delta_{\sigma,s} + \delta_{\sigma,a} - 2\delta_{ref}), \quad (2.21a)$$

$$\delta_{\sigma,-} = \delta_{\sigma,1} - \delta_{\sigma,2} = \frac{1}{2}(\delta_{\sigma,s} - \delta_{\sigma,a}). \quad (2.21b)$$

The Landauer-Büttiker formula describes the relation between conductance g and the phase shift $\delta_{\sigma,-}$. At zero temperature:

$$g = G/G_Q = \frac{1}{2}\sum_\sigma |S_{LR}^\sigma|^2 = \frac{1}{2}\sum_\sigma \sin^2(\delta_{\sigma-}). \quad (2.22)$$

g is normalized by $G_Q = 2e^2/h$ making it dimensionless. Another essential relation in the later calculation is the Friedel sum rule. The number of spin σ electrons bound by the impurity is given in [13] by

$$\left[\frac{1}{2\pi i}\left(\text{Tr}\log S^{\text{full}} - \text{Tr}\log S^{\text{band}}\right) - \left(n^{\text{full}} - n^{\text{band}}\right)\right] \mod \mathbb{Z} = 0, \quad (2.23)$$

where the index full denotes the system with non-zero potential and interaction and band stands for the system without potential. Since interaction reduces to an effective potential in static fRG, we can also take band to be noninteracting. S is the S-matrix and n is the total number of particles in the system. If the band values remain constant, we can simplify this relation to

$$n_\sigma \mod \mathbb{Z} = \frac{\delta_{\sigma,+}}{\pi}. \tag{2.24}$$

2.2.2 Fermi-liquid Theory

The Fermi-liquid theory we introduce in this subsection describes low energy transport properties of a SIAM in terms of a set of Fermi-liquid parameters. Extracting these parameters out of transport properties at low magnetic fields for zero temperature and zero bias voltage will empower us to immediately describe transport at low temperature and low bias voltage.

To introduce the Fermi-liquid parameters, relate them to susceptibilities of the systems, and use them to express transport coefficients of the SIAM, we consider one electron scattering properties of the SIAM. The shift $\delta_{\sigma,-}$ between the symmetric phase and the antisymmetric phase can be expanded in terms of kinetic energy ϵ of the incoming particles and the deviation of the distribution function $\delta n_{\sigma,\epsilon_0} = n_\sigma - n^0_{\epsilon_0}$ around an unphysical reference energy ϵ_0 with distribution function $n^0_{\epsilon_0} = \theta(\epsilon_0 - \epsilon)$ at zero temperature. We will exploit the arbitrariness of ϵ_0 to find relations between the expansion coefficients α_1, ϕ_1, α_2 and ϕ_2, which we call Fermi-liquid parameters.

$$\delta_{\sigma,-}(\epsilon, n_\sigma, n_{\bar\sigma}) = \delta_{0,\epsilon_d-\epsilon_0} + \alpha_{1,\epsilon_d-\epsilon_0}(\epsilon - \epsilon_0) - \phi_{1,\epsilon_d-\epsilon_0} \int_{-\infty}^{\infty} d\epsilon' \delta n_{\bar\sigma,\epsilon_0}(\epsilon') + \alpha_{2,\epsilon_d-\epsilon_0}(\epsilon - \epsilon_0)^2$$

$$- \frac{1}{2}\phi_{2,\epsilon_d-\epsilon_0} \int_{-\infty}^{\infty} d\epsilon'(\epsilon + \epsilon' - 2\epsilon_0)\delta n_{\bar\sigma,\epsilon_0}(\epsilon') - ...$$

$\bar\sigma$ is the spin opposite to σ. Since ϵ_0 is unphysical and arbitrarily chosen, we know that $\partial_{\epsilon_0}\delta(\epsilon, n_{\sigma'}) = 0$. Performing this differentiation and comparing constant terms and coefficients of each $\propto (\epsilon - \epsilon_0)$, $\int_{\epsilon'} \delta n_{\bar\sigma,\epsilon_0}$ and their higher powers yields the following set of useful equations

$$-\frac{d\delta_0}{d\epsilon_d} - \alpha_1 + \phi_1 = 0, \tag{2.25a}$$

$$-\frac{d\alpha_1}{d\epsilon_d} - 2\alpha_2 + \phi_2/2 = 0, \tag{2.25b}$$

$$\frac{d\phi_1}{d\epsilon_d} + \phi_2 = 0. \tag{2.25c}$$

For zero temperature and low magnetic field B, $\delta_{\sigma,-}$ can be expressed by B and the Fermi-liquid parameters: [8]

$$\delta_{\sigma,-}(\mu_\sigma, n^0_{\mu_{\sigma'}}) = \delta_0 + \frac{\sigma}{2}(\alpha_1 + \phi_1)B + \frac{1}{4}(\alpha_2 + \phi_2/4)B^2. \tag{2.26}$$

We can write the charge of the impurity as $n_d = n_{d\uparrow} + n_{d\downarrow}$ and the magnetization as $m_d = n_{d,\uparrow} - n_{d,\downarrow}$. Antisymmetric modes do not interact with a single site impurity. Correspondingly, their phase shift is zero, $\delta_{\sigma,a} = 0$. Via Eq. (2.24) and Eq. (2.21) this leads us to

$$n_\sigma = \frac{\delta_{\sigma,+}}{\pi} = \frac{\delta_{\sigma,-}}{\pi}. \tag{2.27}$$

The charge and spin susceptibilities at $B = 0$ can then be expressed entirely by the Fermi-liquid parameters:

$$\chi_c = -\frac{\partial n_d}{\partial \epsilon_d}\Big|_{B=0} = -\frac{2}{\pi}\frac{\partial \delta_0}{\partial \epsilon_d} = \frac{2}{\pi}(\alpha_1 - \phi_1), \qquad \chi_s = \frac{\partial m_d}{\partial B}\Big|_{B=0} = \frac{1}{2\pi}(\alpha_1 + \phi_1). \tag{2.28}$$

We obtain two more equations by differentiating the susceptibilities with respect to ϵ_d ($\chi'_\alpha = \frac{\partial \chi_\alpha}{\partial \epsilon_d}$). Using Eq. (2.25) and Eq. (2.28) we get:

$$\alpha_1 = \pi(\chi_s + \chi_c/4), \tag{2.29a}$$

$$\alpha_2 = \pi(-\frac{3}{4}\chi'_s - \chi'_c/16), \tag{2.29b}$$

$$\phi_1 = \pi(\chi_s - \chi_c/4), \tag{2.29c}$$

$$\phi_2 = \pi(-\chi'_s + \chi'_c/4). \tag{2.29d}$$

The susceptibilities used to express the SIAM Fermi-liquid parameters can be found by the Bethe ansatz. They are shown in Fig. 2.1. Later we will try to compute the FL parameters for a quantum dot. Here, the susceptibilities will be calculated numerically by using an fRG simulation. Our goal is to describe the conductance behavior for small deviations of the magnetic field, temperature and bias voltage from zero in terms of the FL parameters. For small magnetic fields we can expand the conductance g. We define the transport coefficient c_B proportional to the curvature of g:

$$g = g_0 + \frac{\partial^2 g}{\partial B^2}\Big|_{B=0}B^2 + \mathcal{O}(B^4) =: g_0 - \frac{2e^2/h}{(E^*)^2}c_B B^2 + \mathcal{O}(B^4), \tag{2.30}$$

where $E^* = \frac{\pi}{4\alpha_1}$. g is symmetric under swapping spins and thus there can be no odd powers of B in the expansion. Using Eq. (2.26) and carrying out all the derivatives we find an expression for c_B:

$$c_B = -\frac{\pi^2}{64}\frac{(\alpha_2 + \phi_2/4)\sin(2\delta_0) + (\alpha_1 + \phi_1)^2\cos(2\delta_0)}{\alpha_1^2}. \tag{2.31}$$

The conductance can also be expanded with regard to temperature T and bias voltage V. c_T and c_V are the corresponding curvatures.

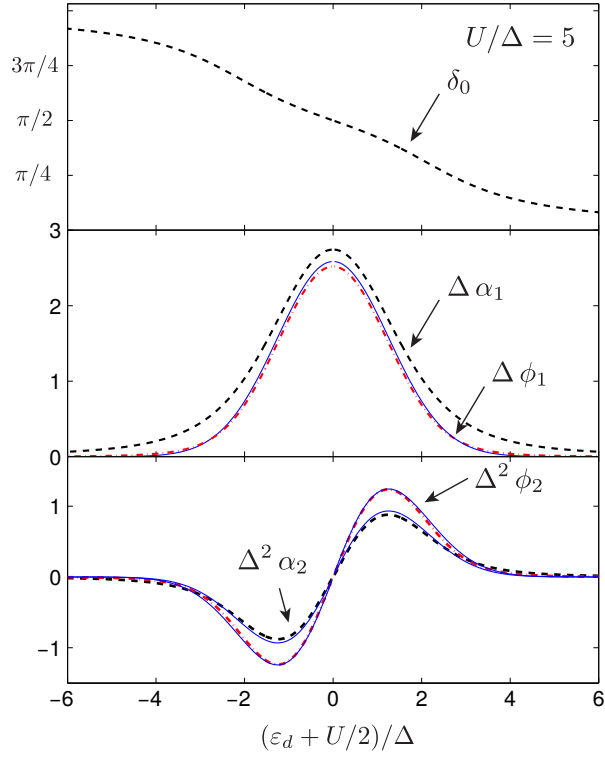$$G(V, T, B) - G_0 \approx -\frac{2e^2/h}{(E^*)^2}\left(c_T T^2 + c_V(eV)^2 + c_B B^2\right). \tag{2.32}$$

Figure 2.1: Fermi-liquid parameters of the SIAM. Figure 1 in Ref. [8]

Similar results to c_B are obtained in for c_T and c_V:

$$c_T = \frac{\pi^4}{16} \frac{\left(\frac{\phi}{12} - \frac{\alpha_2}{3}\right) \sin\left(2\delta_0\right) - \left(\frac{\alpha_2^2}{3} + \frac{2\phi_1^2}{3}\right) \cos\left(2\delta_0\right)}{\alpha_1^2}, \tag{2.33}$$

$$c_V = \frac{\pi^2}{64} \frac{\left(\frac{3\phi_2}{4} - \alpha_2\right) \sin 2\delta_0 - \left(\alpha_1^2 + 5\phi_1^2\right) \cos 2\delta_0}{\alpha_1^2}, \tag{2.34}$$

their derivation will not be repeated here. It can be found in [8].

Chapter 3

Application to the Quantum Dot

3.1 The Quantum Dot

We model the quantum dot (QD) by a special form of potential barrier. In our case, it is of symmetric shape with two maxima on the sides. Their height is varied by the side gate voltage V_s and their spatial position determines the width of the potential well in between. The well is parabolic in the center and its depth is described by the gate voltage V_g. The fRG simulation of the system uses the discretized potential shown in Fig. 3.1

$$P_j = \begin{cases} V_g + 2\tau + \mu + \frac{\Omega_x^2 i^2}{4\tau}\mathrm{sgn}(V_s - V_g), & \text{for } 0 \leq |j| \leq j_0, \\ (V_s + 2\tau + \mu)[2(\frac{|j|-N}{j_s-N})^2 - (\frac{|j|-N}{j_s-N})^4], & \text{for } j_0 \leq |j| \leq N, \\ 0, & \text{for } |j| > N. \end{cases} \qquad (3.1)$$

$2N + 1$ is the total number of sites and $2j_s + 1$ is the distance between the two side gates. The parameters Ω_x and j_s are chosen such that the potential is continuously differentiable. 4τ is the band width. Additional terms of the Hamiltonian are on-site interactions of the electrons and a kinetic hopping term. The interaction is limited to the central region.

$$U_j = \begin{cases} U_0 \exp\left[-\frac{(j/N)^6}{1-(j/N)^2}\right], & \text{for } 0 \leq |j| \leq N, \\ 0, & \text{for } |j| > N. \end{cases} \qquad (3.2)$$
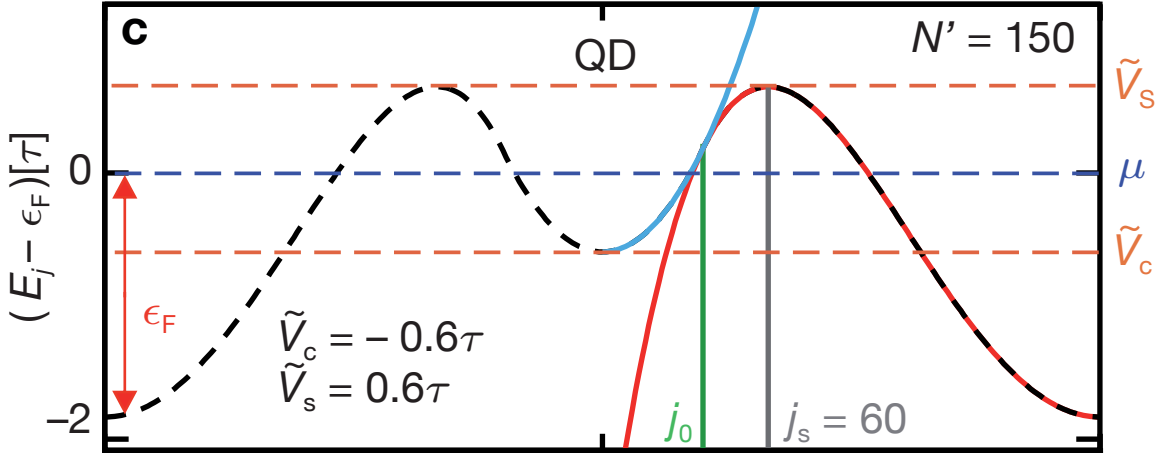
Figure 3.1: The potential of the quantum dot with its parameters. $\tilde{V}_S = V_s$, $\tilde{V}_C = V_g$, $N' = N$. Figure S9c in Ref. [5].

The full Hamiltonian is

$$H = H_{\text{pot}} + H_{\text{hop}} + H_{\text{int}} + H_B, \tag{3.3}$$

$$H_{\text{pot}} = \sum_{i=-\infty}^{\infty} \sum_{\sigma} P_i c_{i\sigma}^\dagger c_{i\sigma}, \tag{3.4}$$

$$H_{\text{hop}} = \sum_{\langle i,j \rangle} \sum_{\sigma} \tau (c_{i\sigma}^\dagger c_{j\sigma} + c_{j\sigma}^\dagger c_{i\sigma}), \tag{3.5}$$

$$H_{\text{int}} = \sum_{i=-\infty}^{\infty} U_i c_{i\uparrow}^\dagger c_{i\uparrow} c_{i\downarrow}^\dagger c_{i\downarrow}, \tag{3.6}$$

$$H_B = -\sum_{i=-\infty}^{\infty} \sum_{\sigma} \frac{B\sigma}{2} c_{i\sigma}^\dagger c_{i\sigma}. \tag{3.7}$$

The functional renormalization group (fRG) implements the concept of a renormalization group flow for interacting quantum many-particle systems. We introduce an infrared cutoff parameter Λ, such that the system can be solved analytically for $\Lambda \to \infty$ and reproduces the full system for $\Lambda \to 0$. Differentiating the generating functional of the one-particle irreducible m-particle vertex functions γ_m with respect to Λ yields an infinite hierarchy of differential equations for the γ_m, so called flow equations. This set of equations is truncated above a certain order of vertices (here $\gamma_m = 0$ for $m \geq 3$, thus some terms of order U_0^3 and higher are neglected). To check if these terms can be disregarded, we compute the maximum value of γ_2, γ_{max}. If it is much bigger than U_0, we cannot guarantee that approximations assuming vanishing of high-order terms in U_0 are valid. Integrating the differential equations and taking the limit $\Lambda \to 0$ yields a numerical solution to the cutoff-free problem [14].

We work with static fRG, where we presume the vertex functions to be constant with respect

to frequency. As a result of the static fRG flow, we obtain a static self energy Σ and a static 2-particle vertex γ_2. We can extract single-particle properties from the effective Hamiltonian

$$H_{\text{eff}} = H_{\text{pot}} + H_{\text{hop}} + H_B + \Sigma. \tag{3.8}$$

Σ may contain long range hopping terms.

The feedback length L is a quantity in fRG that determines how the different channels of the two-particle vertex γ_2 couple. For all following computations we set $N = 30$, $j_0 = 10$, $U_0 = 1$ and $L = 20$.

3.2 SIAM Fermi-liquid parameters for the Quantum Dot

The quantum dot is of course more complicated than the SIAM. Examining its local density of states (LDOS) in Fig. 3.2, we see that multiple levels form in the potential well. The transport properties are mainly determined by the level closest to the chemical potential μ (Fig. 3.3). Landauer-Büttiker formula yields maximal conductance, when a level is half occupied, i.e. when the level crosses the chemical potential. The lower levels remain fully occupied. Their contribution can be absorbed in an extra energy term Σ_{lower}. If the change in the upper level has only a small impact on the lower levels, the interaction Σ_{lower} can be considered constant.

It turns out to be succesful, if we treat this upper level like the impurity level in a SIAM. In this work we examined its Fermi-liquid properties following two different approaches. Approach (A) attempts to assign an effective SIAM level position ϵ_d to the QD system and varies V_g. Approach (B) determines the Fermi-liquid parameters by varying μ.

Later we will compare the results for the magnetic transport coefficient obtained by using the Fermi-liquid parameters and Eq. (2.31) to computing it directly from the curvature of the conduction for small magnetic fields.

3.2.1 Phases in the Quantum Dot

In the SIAM electrons interact on a single site. Thus particles with antisymmetric wave functions experience no phase shift. This is different for the QD. When electrons scatter off an antisymmetric level at the chemical potential, the symmetric phase δ_s is zero or an integer multiple of 2π (Fig. 3.4).

The derivation of the SIAM transport properties was limited to symmetric scattering, but can be modified to give a very similar result for antisymmetric scattering.

In Eq. (2.27), $\delta_s = 0$ results in an extra minus sign

$$n_\sigma = \frac{\delta_{\sigma,+}}{\pi} = -\frac{\delta_{\sigma,-}}{\pi}. \tag{3.9}$$

This change results in an extra minus sign for all Fermi-liquid parameters. $\delta_0 = (\delta_s - \delta_a)/2$ is also changing sign if we switch the roles of the phases. The transport coefficients do not change sign, because the formulas contain an even number of sign changing factors in each term.
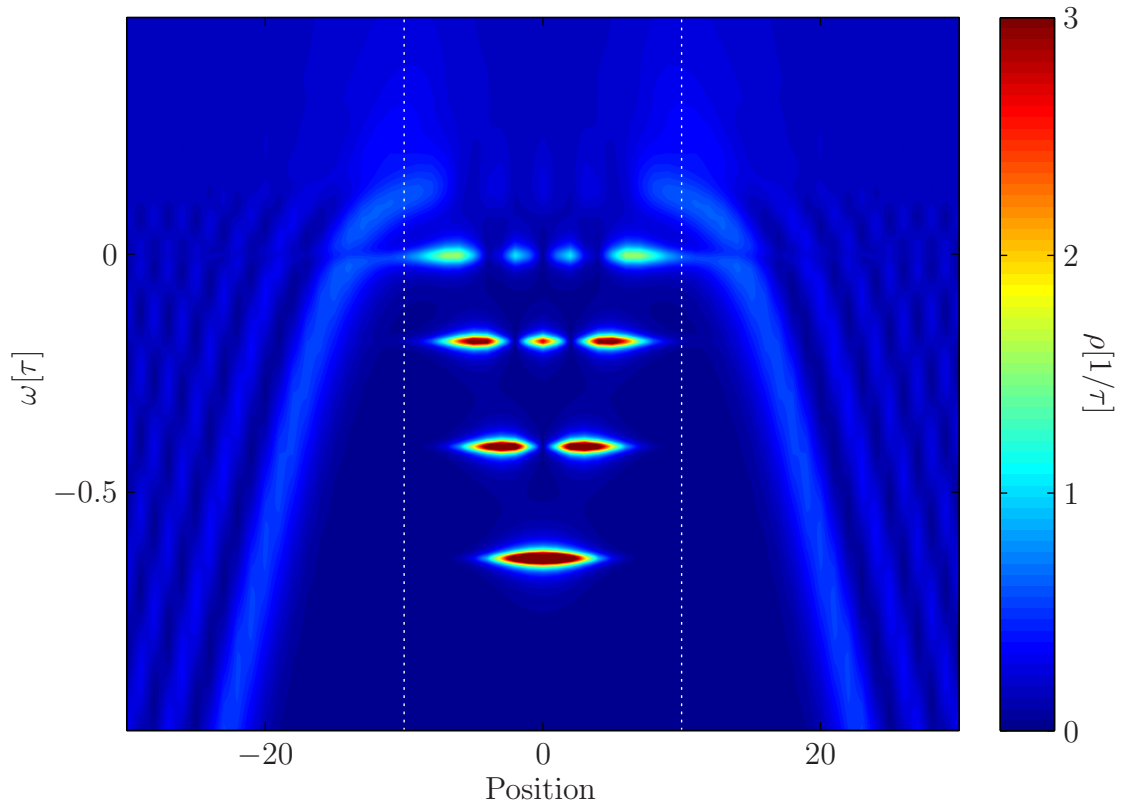
Figure 3.2: The LDOS of an interacting QD with $V_g = -1\tau$, $V_s = 0.01\tau$ and $\mu = 0\tau$ is plotted here for varying energies ω relative to the middle of the band. We can see localized levels in the central region (sites -10 to 10, white dotted line). Each level below the chemical potential is occupied by one spin-up and one spin-down electron. Lower lying levels can have a high lifetime leading to a very small linewidth. These levels can be missed if the stepwidth in ω is too big. We artificially reduce the lifetime by adding a small imaginary part $i\delta$ to the frequency in the Green's function. Thus the levels appear broader. Here $\delta = 1/100$.
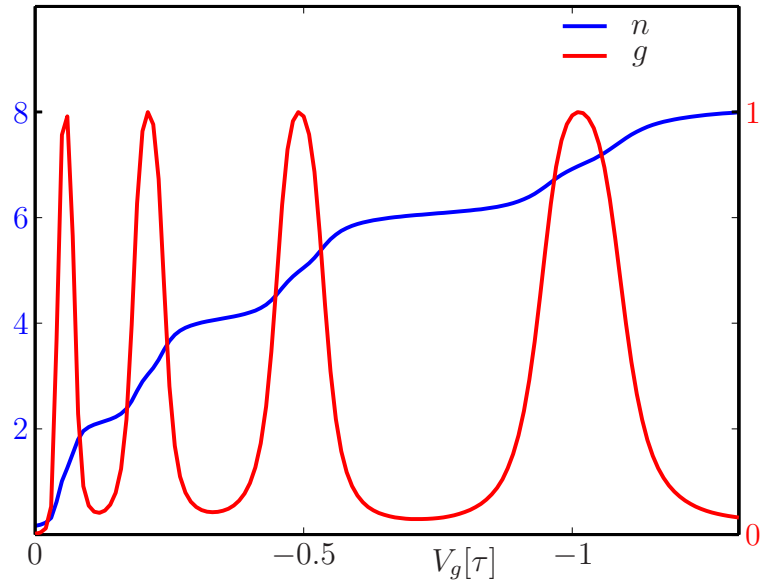
Figure 3.3: We vary V_g of an interacting QD with $V_s = 0.01\tau$. Every time a level is moved above the chemical potential $\mu = 0$, the two electrons on it are released. Thus the occupation number is a step function with plateaus at every even value. The conductance g is low, when the occupation number remains constant, but has peaks, when the occupation number changes.
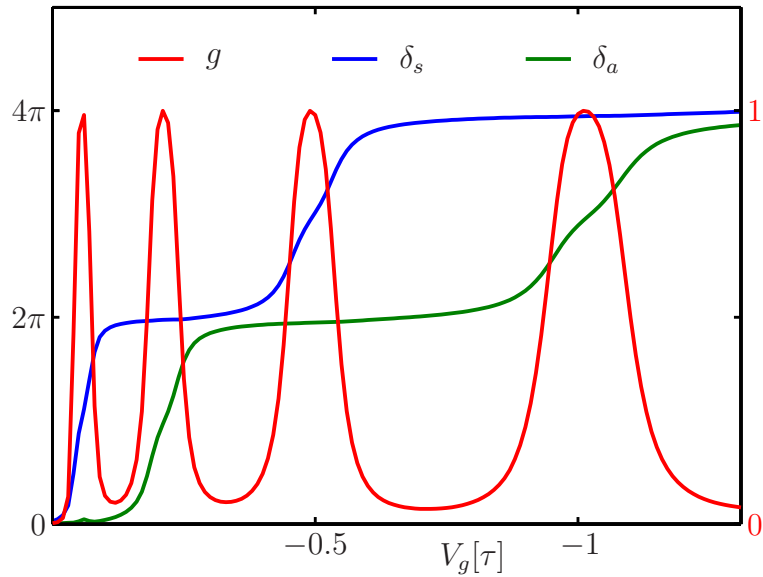
Figure 3.4: At each conductance peak, one phase makes a 2π step. The other stays constant. δ_s changes, when the conducting level has a symmetric wave function. δ_a changes, when the conducting level has an antisymmetric wave function.

3.2.2 (A) Effective level position

We want to apply the previous Fermi-liquid calculations to the quantum dot. However, it is not sufficient to determine the level position in the LDOS for the fully interacting system, because it already factors in the interaction on the upper level. This interaction would be twice accounted for if we were to use this level position in the SIAM Hamiltonian where there is an extra term for the interaction on the conducting level. We find an effective level position by considering a chemical potential $\tilde{\mu}$ sufficiently below the upper level such that all lower levels are occupied (see Fig. 3.5). Only they contribute to the self energy $\Sigma_{\tilde{\mu}}$ of the system with chemical potential $\tilde{\mu}$. We now construct an effective Hamilonian without shifted level position due to the interaction in the upper level

$$H_{\mathrm{eff}} = H_{\mathrm{pot}} + H_{\mathrm{hop}} + \Sigma_{\tilde{\mu}}. \tag{3.10}$$

When we look at the LDOS resulting from H_{eff} we can read off the effective level position ϵ_d. In a previous examination of the QD, Ref. [9] determined ϵ_d by computing the local density of particles in the lower levels for $\tilde{\mu}$ and acquiring H_{eff} by adding a resulting Hartree shift to the upper level. The method used here includes the Hartree shift, but also takes interactions of higher order involving the lower levels into account. To compute the Fermi-liquid parameters over a range of ϵ_d, we vary V_g and find $\epsilon_d(V_g)$. As seen in Fig. 3.6, ϵ_d is a linear function of V_g.

When we need to differentiate an arbitrary quantity A by ϵ_d in Eq. (2.29) we simply use the chain rule

$$\frac{\partial A}{\partial \epsilon_d} = \frac{\partial A}{\partial V_g} \left(\frac{\partial \epsilon_d}{\partial V_g} \right)^{-1}, \tag{3.11}$$

which effectively is a multiplication by a constant here. The susceptibilities are calculated from the densities given by the fRG program at varying V_g and small B. The occupation of the upper level and the scattering phases are shown in Fig. 3.8. We see, how the occupation number decreases by two, when the level rises above the chemical potential. δ_s remains constant, while δ_a goes from 2π to 0. It is essential for the comparison to the SIAM that one phase can be considered constant at the conductance peak, so that Eq. (2.27) is satisfied. We can now calculate the Fermi-liquid parameters and subsequently the transport coefficients. The resulting Fermi-liquid parameters obtained by this approach can be seen in Fig. 3.9. Compared to the values for the SIAM in Fig. 2.1 the QD demonstrates a slight asymmetry. This is expected, because the QD is not a perfectly symmetric system like the SIAM. The fraction U/Δ describes the strength of the interaction. When well is made more shallow, the tunneling rate and thus the hybridization Δ increases significantly (Fig. 3.7), leading to an effective decrease in interaction strength. This feature is completely absent for a SIAM in the wide band limit. The transport coefficients that were computed by Eq. (2.31) and Eq. (2.33) are shown in Fig. 3.2.2. We can compare the c_B from our FL calculation to the curvature of the conductance we determine directly from the fRG data. This is a good test of the validity of our model. Figure 3.11 shows good agreement in the central region, but large deviation on the sides of the plot, corresponding to the mixed-valence regime, where the determination of the effective level position described above presumably becomes unreliable. We can argue that the differences on the sides are exaggerated by a factor of $\frac{1}{\alpha_1^2}$, where $\alpha_1 \to 0$. We can see in Eq. (2.30), that the curvature of g is proportional to $\tilde{c}_B \alpha_1^2$. Figure 3.12 shows agreement between the FL and fRG results for $\tilde{c}_B$.
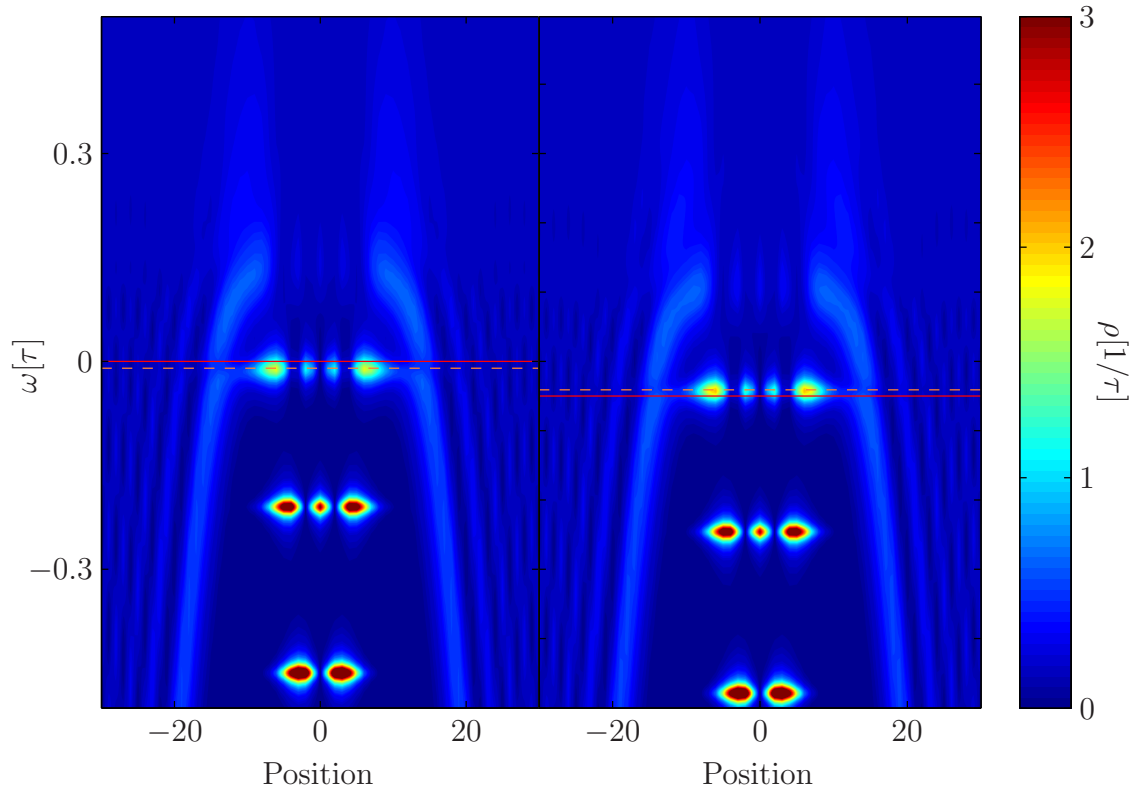
Figure 3.5: LDOS of an interacting QD with $V_g = -1.1\tau$ and different chemical potentials indicated by the red solid line. For this and all of the following figures in (A) we set $V_s = 0.01\tau$. The energy ω is measured relative to the middle of the band. On the left side (for chemical potential $\mu = 0\tau$), the level is occupied and its position is higher than that of the right side, where the upper level is unoccupied (chemical potential $\tilde{\mu} = -0.05\tau$). The difference lies in the interaction of the electrons in the upper level. The position of the upper level (dashed orange line) for the chemical potential $\tilde{\mu}$ is what we determine to be the effective level position.
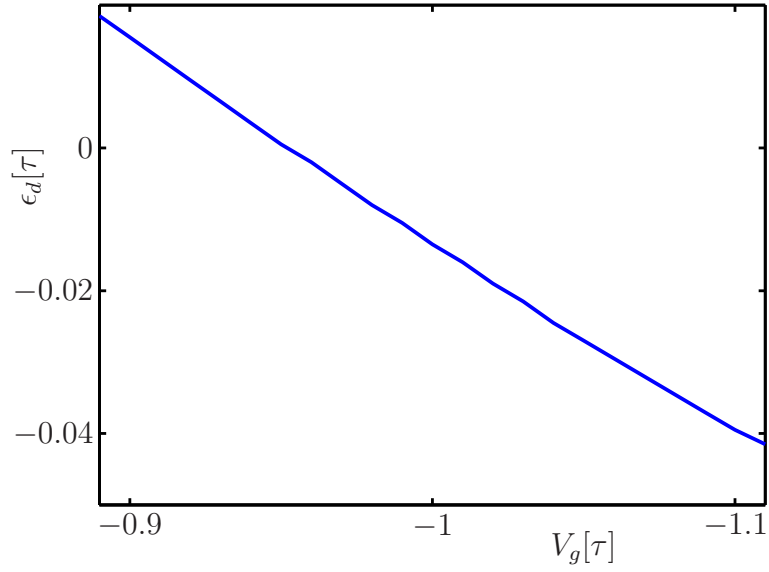
Figure 3.6: ϵ_d is determined for a range of V_g. ϵ_d is linear with a slope of approximately 0.25.
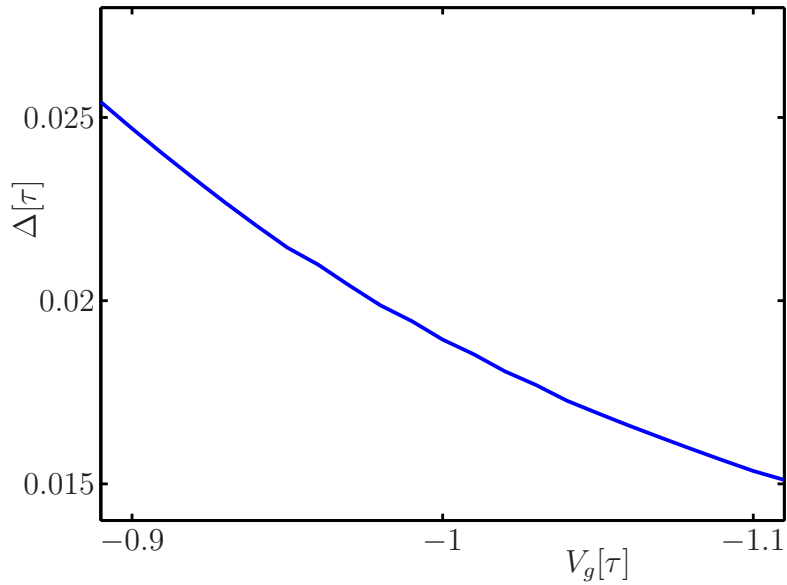
Figure 3.7: The hybridization Δ was determined by fitting a Lorentzian function to the upper level at chemical potential $\tilde{\mu}$. $\Delta = \Gamma/2$, where Γ is the linewidth of the Lorentzian. In the following, we set the Δ to its value at the conductance peak, $\Delta(V_g = 0.98) = 0.0181$.
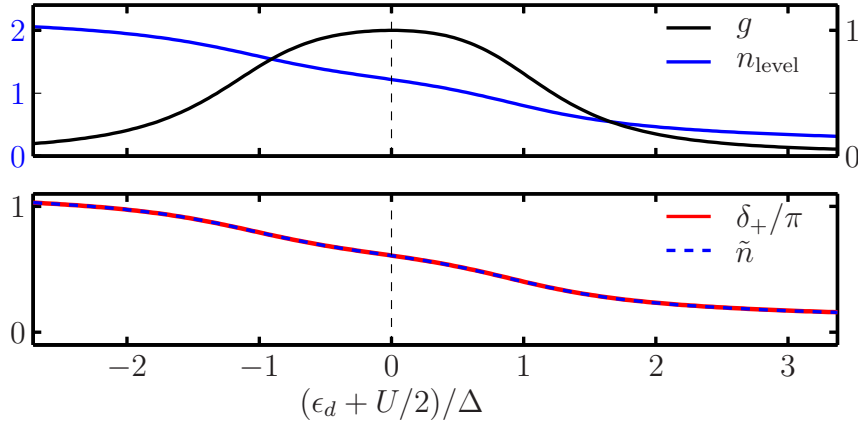
Figure 3.8: We show the total number $n = n_\uparrow + n_\downarrow$ of electrons in the system and the phases δ_a and δ_s close to the resonance, where the conductance g has a peak. We plot $\tilde{n} = (n_\sigma)_\mathbb{Z}$ and δ_+/π to demonstrate the validity of the Friedel sum rule.
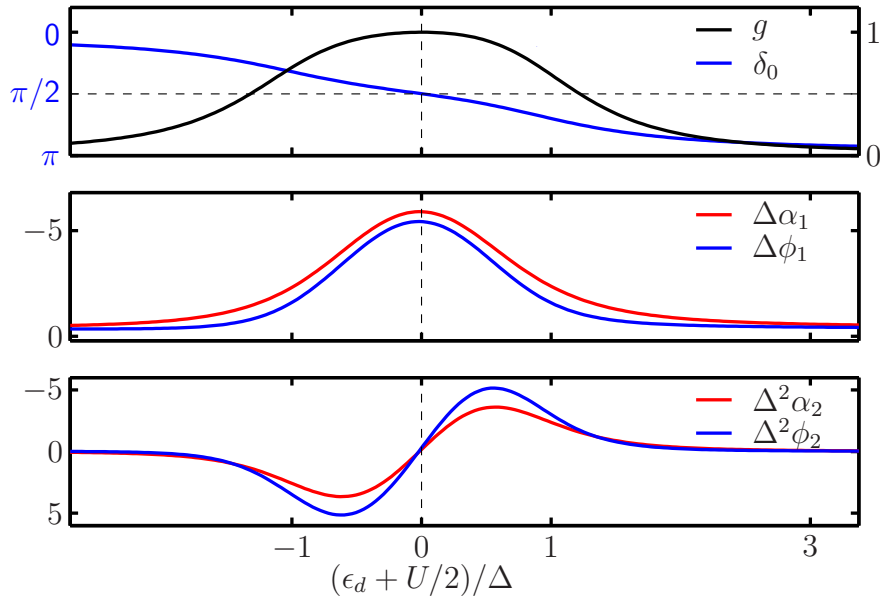
Figure 3.9: Fermi-liquid parameters determined for effective level positions. In the SIAM, at the particle-hole symmetric point, $\epsilon_d = U/2$ is fulfilled, when $\mu = 0$. Also, $\alpha_2 = \phi_2 = 0$. We seek out the point, where $\alpha_2 = \phi_2 = 0$ and apply the symmetry condition to find $U = 1.9\Delta$ for the QD used here. Here, we considered a bound state with antisymmetric wave function. As discussed in 3.2.1, all quantities except conductance switch sign. To preserve comparability to the SIAM, we flip the y-axes of these quantities.
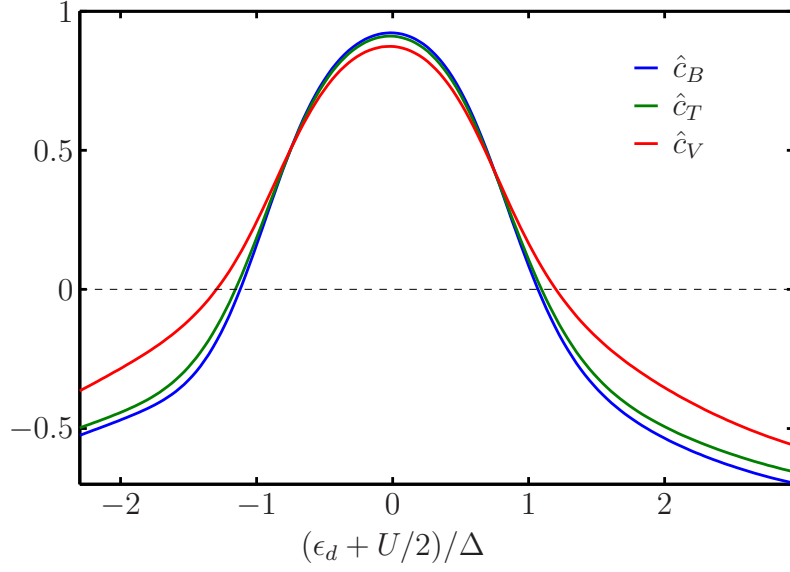
Figure 3.10: Normalized transport coefficients for magnetic field (blue), temperature (green) and bias voltage (red). The same normalization as in [8] was used: $\hat{c}_\alpha = c_\alpha/c_\alpha^K$ with $c_B^K = \frac{\pi^2}{16} \approx$ 0.617, $c_T^K = \frac{\pi^4}{16} \approx 6.009$ and $c_V^K = \frac{3\pi^2}{32} \approx 0.925$. Similar to the Fermi-liquid parameters for the QD, these curves are not symmetric in ϵ_d.
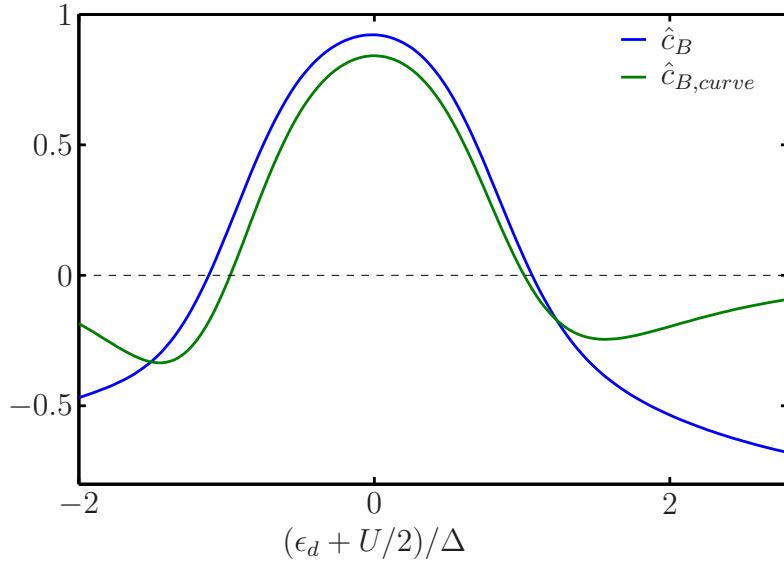

Figure 3.11: Normalized transport coefficient for magnetic field. Comparison of the Fermi-liquid calculation to the data from the fRG simulation.
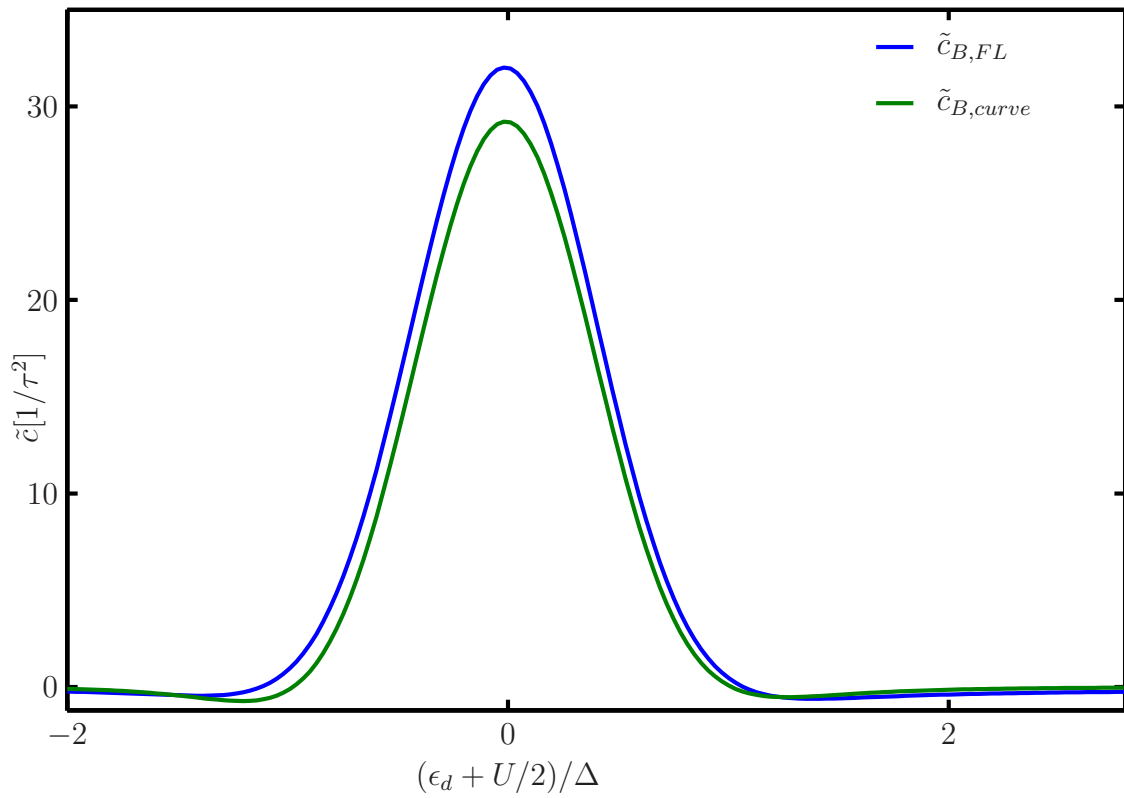
Figure 3.12: The results of Fig. 3.11 without the normalization: $\tilde{c}_B = c_B \cdot \alpha_1^2$.

3.2.3 (B) Chemical potential

We consider the wide band limit, where every energy can be considered far away from the bands bottom and top and change in distances relative to band limits are disregarded as small. No physical quantity in the SIAM can depend just on the absolute value of ϵ_d or μ because the energy can have an arbitrary offset. They should only depend on the difference $\epsilon_d - \mu$. It is the same for the QD as long as we do not change the shape of the potential. This enables us to rewrite the differentiation of any physical quantity A as

$$\frac{\partial A}{\partial \epsilon_d} = -\frac{\partial A}{\partial \mu}. \tag{3.12}$$

Thus, we can vary the chemical potential instead of the gate voltage. This is very promising since it leaves the shape of the potential unchanged and is conceptually simpler. We first look at a QD with $V_s = 0.06\tau$ and vary μ in steps of $2 \cdot 10^{-3}$ around the upper level as seen in Fig. 3.13.
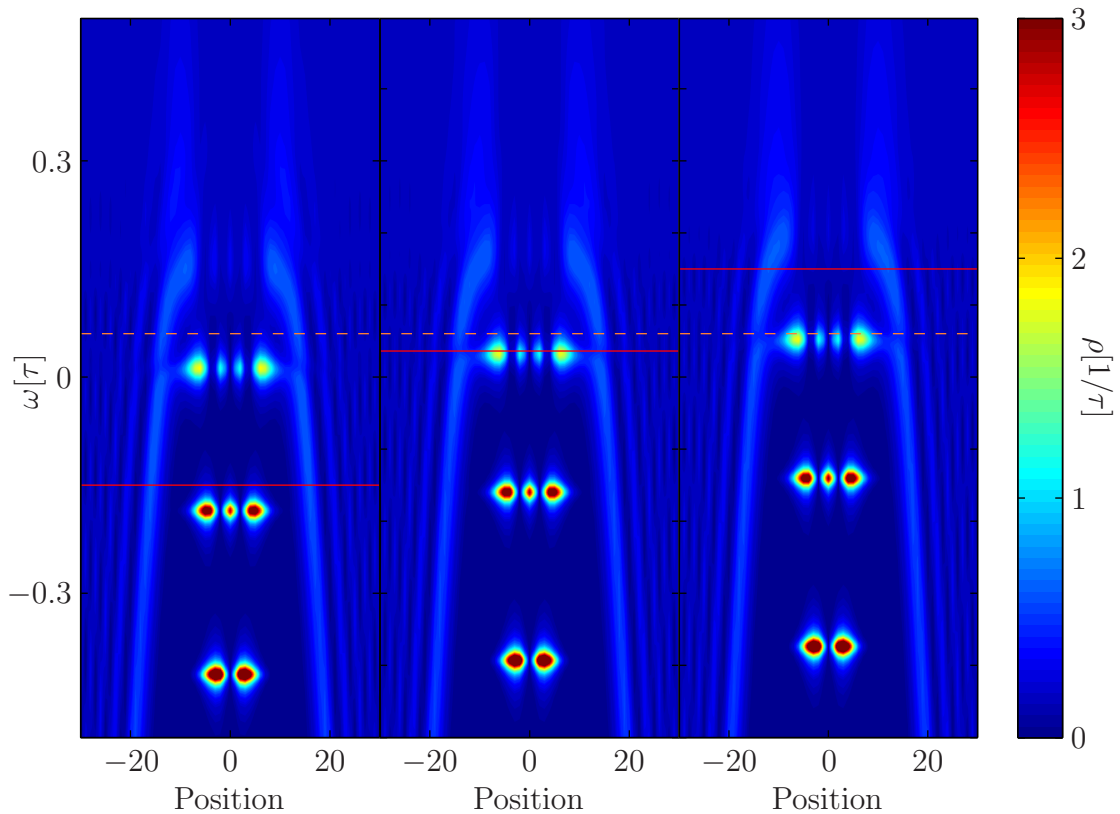

Figure 3.13: We vary μ (solid line) from below to above the upper level and observe how its energy is raised by being occupied. The level can rise above V_s (dashed line). ω is measured relative to the center of the band here.
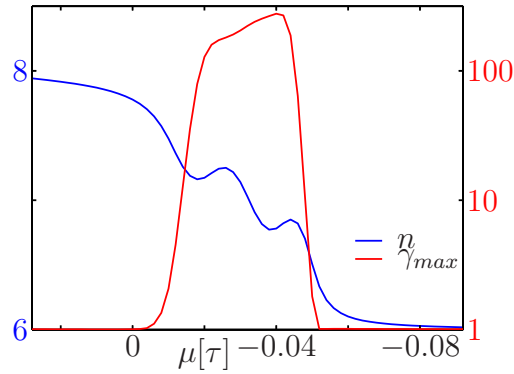
Figure 3.14: The occupation number of the QD n shows faulty behavior for $V_g = -1.25\tau$ as a function of μ. It should be monotonous as μ passes the level. If we plot γ_{max} logarithmically, we see that γ_2 has entries much bigger than $U_0 = 1$. This makes the approximations used by fRG invalid, as seen in subsection 3.1.

When choosing a level we want to examine, we need to be careful, that the level will not rise above the side gates on the right side of Fig. 3.13 as the level will only be partially occupied. This is an extra detail that is implicit in (A) where the fixed chemical potential is always below the side gates. On the other hand, the fRG program could not handle levels that were too deep, because they were too narrow to solve. This can be seen in Fig. 3.14.

Another detail that was not present in (A) is an extra phase shift that is linear in the change of μ. We can see this in Fig. 3.15. If we vary the gate voltage of the QD, the change is localized to the central region. The change in chemical potential is not local, but also effects electrons outside of the QD.
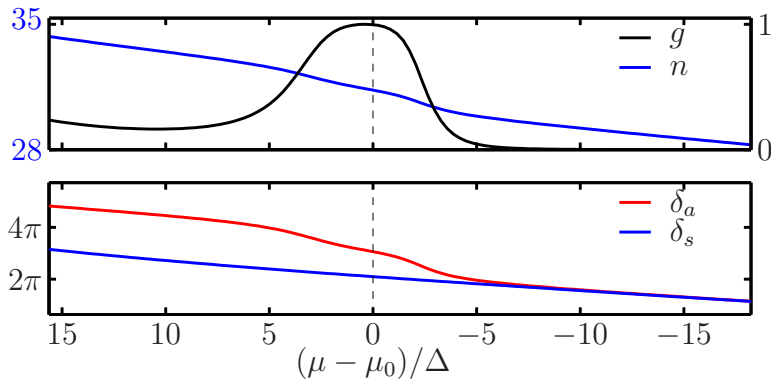

Figure 3.15: We see that the total number of electrons n in the system is not constant away from the conductance peak, but steadily increases with μ. The phases δ_a and δ_s show the same behavior. The conductance g does not go to zero for $\mu > \mu_0$. We will later detail, why the Anderson model cannot be applied when the chemical potential is above the side barriers.
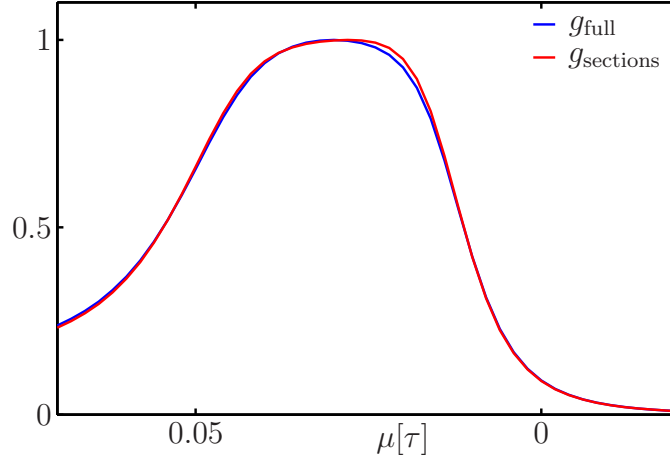
Figure 3.16: The conductance of a system with the sectioned Hamiltonian shows close resemblance to the conductance of the full system. The relative deviation in the peak area is at most 3%.

Reduction to central region

To remove the impact of the sides, we try to reduce the system to the central region. We split the entire QD potential in three parts: left side, center, right side. The division is made at the side gate maxima. The Hamiltonian of the full system from the fRG computation allows long range hopping between all parts. We only want to allow short range hopping between the three sections, effectively extending the leads to the maxima of the barriers. We thus set all other hopping terms between different sections to zero to obtain a new Hamiltonian H_{block}

$$H_{\text{block}} = \begin{pmatrix} H_{\text{left}} & \begin{matrix} 0 & \cdots & 0 \\ \vdots & \ddots & \vdots \\ \tau & \cdots & 0 \end{matrix} & 0 \\ \begin{matrix} 0 & \cdots & \tau \\ \vdots & \ddots & \vdots \\ 0 & \cdots & 0 \end{matrix} & H_{\text{center}} & \begin{matrix} 0 & \cdots & 0 \\ \vdots & \ddots & \vdots \\ \tau & \cdots & 0 \end{matrix} \\ 0 & \begin{matrix} 0 & \cdots & \tau \\ \vdots & \ddots & \vdots \\ 0 & \cdots & 0 \end{matrix} & H_{\text{right}} \end{pmatrix} \tag{3.13}$$

We compare the conductance of the system with the full Hamiltonian to that of the sectioned system in Fig. 3.16. We see, that only allowing short range hopping between the sections is a reasonable simplification of the system.

 Now we can use the S-matrix formalism seen earlier and apply it to the reduced central system. The leads are extended to the maxima of the barriers. Following this, we need to make adjustments to the the quantities in Eq. (2.19). $\rho_c^\sigma(\omega = \mu)$ is no longer the LDOS at the end of
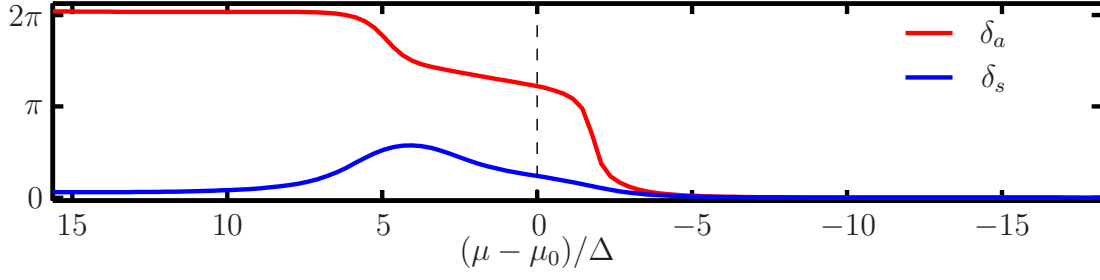
Figure 3.17: Symmetric and antisymmetric phases δ_s and δ_a, if the system is reduced to the central region of the QD. We could eliminate the phase shift from the sides, but the phases are not what we expected, as δ_s is not constant in the peak region and δ_a is asymmetric. We suspect that this behavior stems from the fact that the incoming and outgoing waves are not plane waves as the effect worsened when we reduced the system even more.

the half infinite chain discussed in the beginning, but also has to account for the potential of the barriers. We compute the LDOS with

$$\rho_c^\sigma(\omega) = -\frac{1}{\pi} \operatorname{Im}(G_{cc}^{\sigma,R}), \tag{3.14}$$

where c is the index of the barrier maximum. $G_{ij}^{\sigma,R}$ is the Green's function

$$G^{\sigma,R} = \frac{1}{\omega - H_{\text{left/right}} + i0^+}, \tag{3.15}$$

The system is symmetric and ρ_c^σ is the same at the left and the right barrier.
We obtain the S-matrix from Eq. (2.19), where l and r are the indices of the left- and rightmost sites of the central region. The resulting S-matrix can be examined like before, giving the phases δ_a and δ_s to compute the FL parameters.
We show the phases in Fig. 3.17. The symmetric phase δ_s exhibits behavior that is very different from being constant, which we would expect. We see the S-matrix phases of the system reduced to the central region. Here, we need to be careful of the intuition we put into the S-matrix. The in- and out-states are not plane waves and are still subjected to the potential on the outside of the barriers. To see that the irregular behavior in Fig. 3.17 is not an effect of varying μ, but of reducing the system to the central region, we can reproduce this effect for varying V_g in Fig. 3.18. The results will not be used for further calculation, because the effects at the resonance are not fully understood. However, the behavior away from the resonance is constant. The extra phase shift of the full system could be removed by only considering the central region. This lets us examine the full system with the understanding that the linear phase shift is a trivial effect from the sides of the QD.
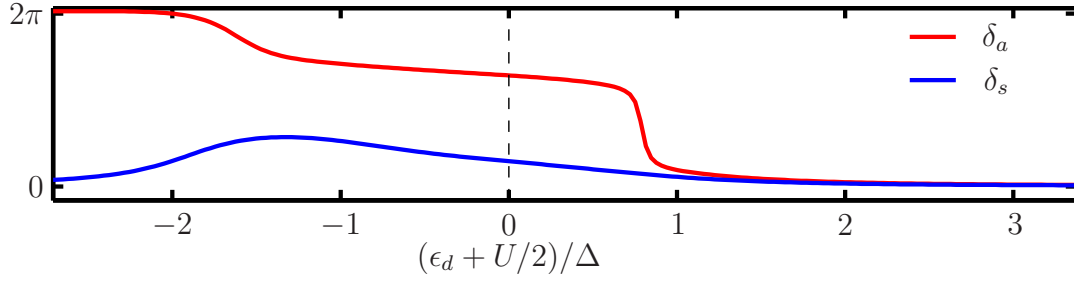
Figure 3.18: Symmetric and antisymmetric phases δ_s and δ_a for varying V_g, if the system is reduced to the central region of the QD. We could reproduce the same problems as in Fig. 3.17 with fixed μ.
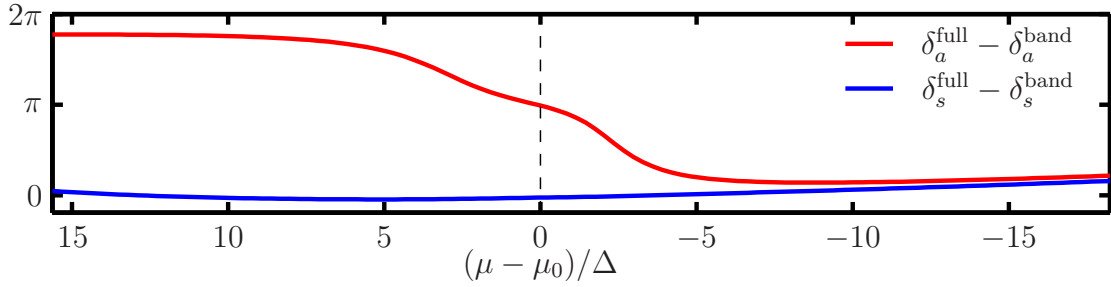

Figure 3.19: The phase differences between the full system and the band system.

Using the full form of the Friedel sum rule

To get rid of the linear shift, we use the full form of the Friedel sum rule and each substract the particle number and the phases of a noninteraction system with zero potential from the respective quantities of the full system. The band values of Eq. (2.23) were constant in (A), but change with μ. The phase differences are shown in Fig. 3.19

To appropiately treat the system as a SIAM, Eq. (2.27) has to be fulfilled. We plot both sides in Fig. 3.20. The relation is sufficiently satisfied up to the side gate voltage, but breaks down at higher μ. At this point, the description of the system by one phase breaks down. We plot the FL parameters in Fig. 3.21. We see that the FL parameters behave similarly to the parameters found in (A). The conductance is asymmetric and does not go to zero. The transport coefficients are plotted in Fig. 3.22.
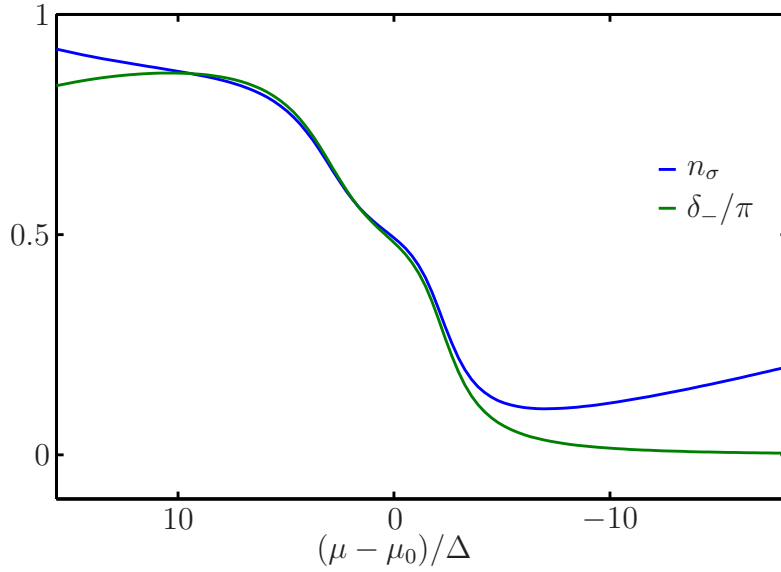
Figure 3.20: Both sides of Eq. (2.27), when the contribution of the band is substracted. We see that the relation is intact at the conductance peak. It breaks down when μ rises above the side gates, where both phases behave nontrivially, and for lower μ, when lower levels begin to matter.
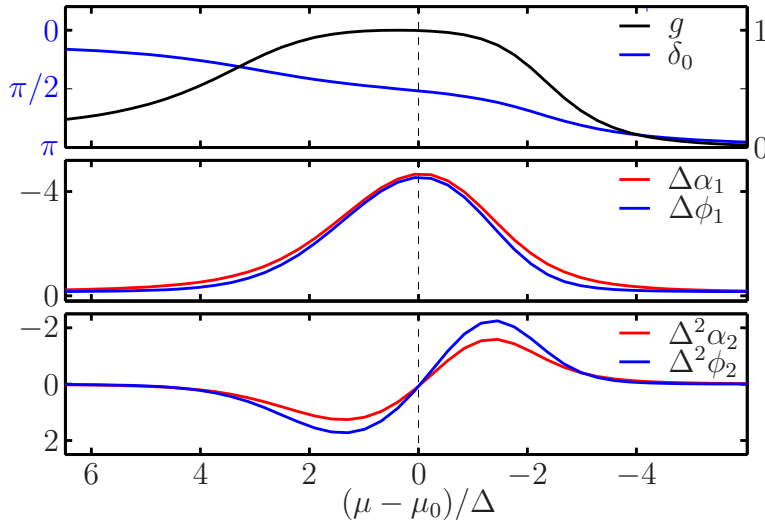

Figure 3.21: Fermi-liquid parameters for varying μ. The hybridization is now smaller than in (A) ($\Delta = 0.0066\tau$), because the side gate voltage is higher ($V_s = 0.06$) and tunneling is exponentially reduced by the height of the barrier. $\mu = \mu_0$ corresponds to the particle-hole symmetric point of the SIAM. From μ_0, we can find U by the relation $\mu_0 - \epsilon_{d,\mathrm{bare}} = U/2$. Here, the interaction is found to be $U = 4.0061\tau$. A bound state with antisymmetric wave function was considered here. As before, we flip the y-axes of all quantities except g.
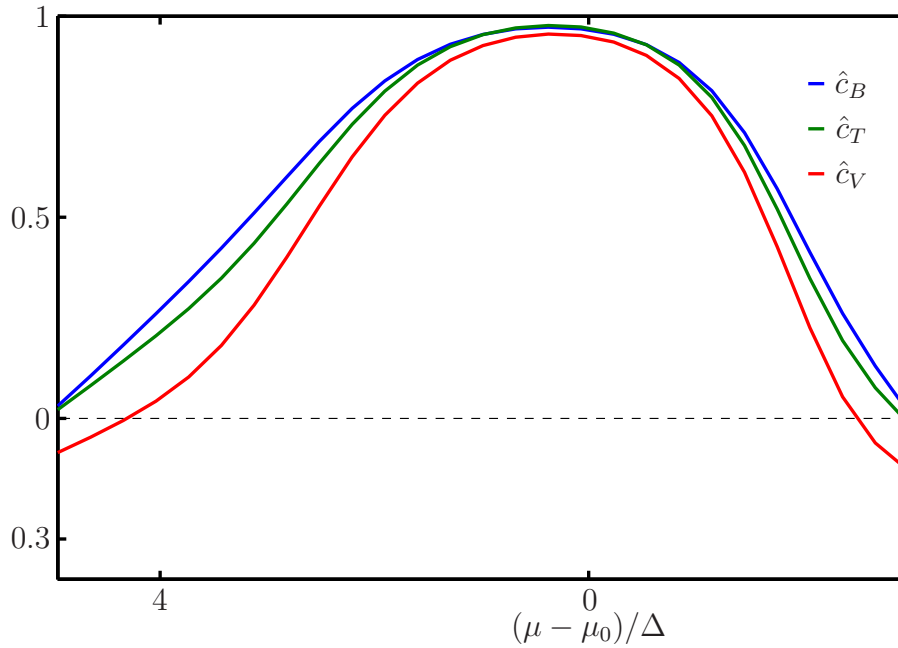
Figure 3.22: Transport coefficients for varying μ.

3.2.4   Comparing both approaches

Both approach (A) and approach (B) qualitatively reproduce the SIAM. To see if (B) is really equivalent to (A) we want to compare them in a single plot. For this, we examine the same Kondo peak we considered in (A). Over a range of V_g, we vary μ and the magnetic field in small intervals around zero at each gate voltage. This way we compute the susceptibilities and subsequently the FL-parameters and transport coefficients. The results for the Fermi-liquid parameters are shown in Fig. 3.23. α_1 and ϕ_1 show good quantitative agreement between both approaches. α_2 and ϕ_2 are only qualitatively similar. We could expect this kind of discrepancy, because α_2 and ϕ_2 depend on second derivatives of with respect to μ and the sampling size was only three values of μ. The necessary data can easily obtained, but the results for the transport coefficients are not very sensitive for the exact form of α_2 and ϕ_2. This can be seen when we plot the results for the transport coefficients in Fig. 3.24. Here, both approaches show good agreement. The deviation between both approaches is shown in Fig. 3.25. Its absolute value is no more than 0.04 in the central region. The relative error would exaggerate the error because all three quantities cross 0. Since all three quantities are of scale 1, we decided that the absolute error would be an appropriate measure of the deviation.
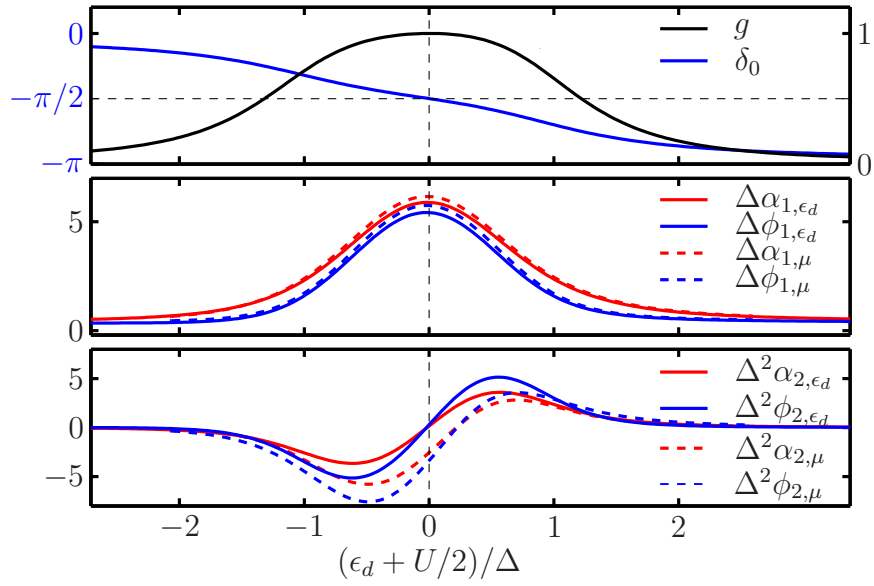
Figure 3.23: Comparison of the Fermi-liquid parameters obtained by approaches (A) (ϵ_d-subscripts) and (B) (μ-subscripts).
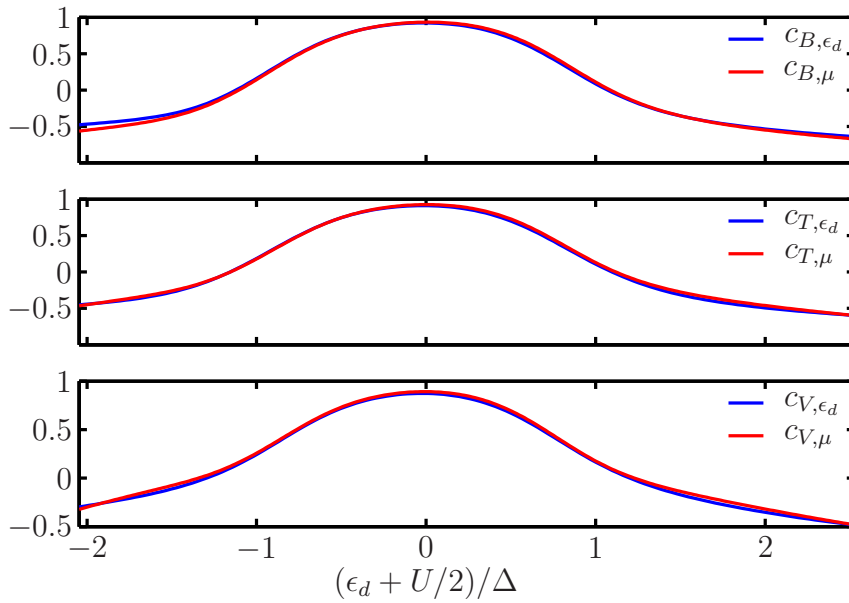

Figure 3.24: Comparison of the transport coefficients obtained by approaches (A) (ϵ_d-subscripts) and (B) (μ-subscripts).
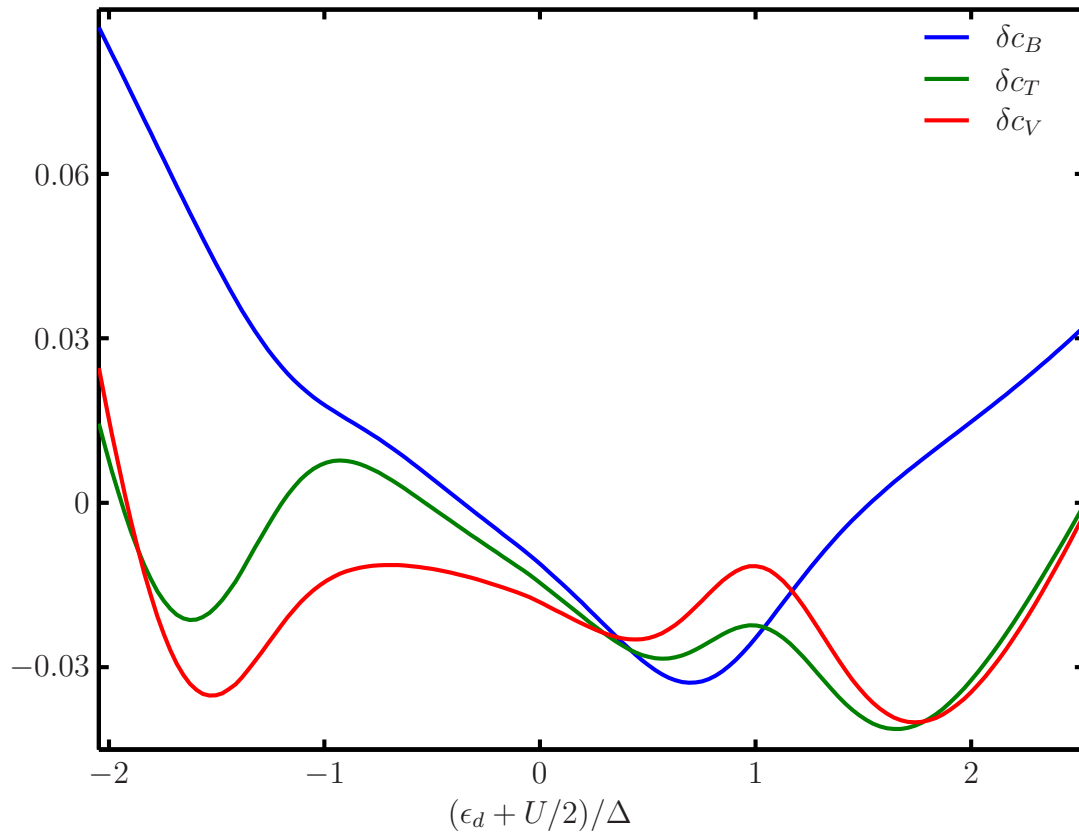
Figure 3.25: Deviation of approaches (A) and (B), $\delta c_\alpha = c_{\alpha,\epsilon_d} - c_{\alpha,\mu}$.

Chapter 4

Conclusion

In this thesis, we applied the Fermi-liquid description of a SIAM to a Quantum Dot potential to compute transport properties at low energies via relations taken from [8]. We explored two approaches, (A) finding an effective level position for a given potential and (B) varying the chemical potential of the system. For (A), we expanded on Philipp Rosenbergers Bachelor thesis, finding a more elaborate way to determine the effective level postition. We computed the Fermi-liquid parameters and transport coefficients for small magnetic fields, temperature and bias voltage. The magnetic transport coefficients were successfully compared to the respective transport coefficient taken directly from fRG data. One problem we encountered, was that the hybridization of the level is not constant when we vary the gate voltage. Introducing an effective level position that is not physically realized is also very artificial. It is favourable to describe the system independent of this. With approach (B), we could escape some of the problems faced in approach (A). We could compute FL parameters and transport coefficients for a varying chemical potential. We compared the results to those of approach (A) and saw that describing the QD by varying the chemical potential is valid, if we are careful of certain things: (1) The upper level position is pinned to the chemical potential, when μ passes the high conductance range. This means that the level can rise above the side gate voltage resulting in an only partially occupied level. If we set the QD too deep in an effort to keep the level below the side gate voltage, the fRG results can become inaccurate. We expect, that this problem could be circumvented in a modified potential. If the side barriers are very narrow, tunneling becomes greater and the fRG could yield valid results. (2) Changing the chemical potential results in a global phase shift. We need to utilize the full form of the Friedel sum rule. (3) When μ is big, both phases of the S-matrix become important and the single phase description taken from the SIAM breaks down. Applying the Fermi-liquid description to the QD without assigning an effective level position is a useful advancement. In systems like the Quantum Point Contact (QPC) no bound states exist and we will need to use this description once a FL-theory exists for the QPC.

Bibliography

[1] L. Jacak, P. Hawrylak, and A. Wojs. *Quantum Dots*. NanoScience and Technology. Springer Berlin Heidelberg, 2013.

[2] L.L. Sohn, L.P. Kouwenhoven, and G. Schön. *Mesoscopic Electron Transport*. Nato Science Series E:. Springer Netherlands, 1997.

[3] Knill E., Laflamme R., and Milburn G. J. A scheme for efficient quantum computation with linear optics. *Nature*, 409(6816):46–52, jan 2001. 10.1038/35051009.

[4] Guido Burkard, Daniel Loss, and David P. DiVincenzo. Coupled quantum dots as quantum gates. *Phys. Rev. B*, 59:2070–2078, Jan 1999.

[5] Bauer Florian, Heyder Jan, Schubert Enrico, Borowsky David, Taubert Daniela, Bruognolo Benedikt, Schuh Dieter, Wegscheider Werner, von Delft Jan, and Ludwig Stefan. Microscopic origin of the /'0.7-anomaly/' in quantum point contacts. *Nature*, 501(7465):73–78, sep 2013.

[6] P. W. Anderson. Localized Magnetic States in Metals. *Phys. Rev.*, 124:41–53, Oct 1961.

[7] P. Nozières. A "fermi-liquid" description of the Kondo problem at low temperatures. *Journal of Low Temperature Physics*, 17(1):31–42, 1974.

[8] Christophe Mora, Cătălin Pa şcu Moca, Jan von Delft, and Gergely Zaránd. Fermi-liquid theory for the single-impurity Anderson model. *Phys. Rev. B*, 92:075120, Aug 2015.

[9] Philipp Rosenberger. Application of a Fermi-liquid theory for the SIAM on an fRG-approach for the description of quantum dots. Master's thesis, LMU Munich, 2015.

[10] J.R. Taylor. *Scattering Theory: The Quantum Theory of Nonrelativistic Collisions*. Dover Books on Engineering. Dover Publications, 2012.

[11] Severin Georg Jakobs. *Functional renormalization group studies of quantum transport through mesoscopic systems*. PhD thesis, RWTH Aachen University, 2009.

[12] Matias Zilly. *Electronic conduction in linear quantum systems*. PhD thesis, University Duisburg, Duisburg, Essen, 2010. Duisburg, Essen, Univ., Diss., 2010.

[13] J. S. Langer and V. Ambegaokar. Friedel Sum Rule for a System of Interacting Electrons. *Phys. Rev.*, 121:1090–1092, Feb 1961.

[14] C. Karrasch. Transport Through Correlated Quantum Dots – A Functional Renormalization Group Approach. *eprint arXiv:cond-mat/0612329*, December 2006.

Acknowledgements

Eidesstattliche Erklärung zur Bachelorarbeit

Hiermit erkläre ich, die vorliegende Arbeit selbständig verfasst zu haben und keine anderen als die in der Arbeit angegebenen Quellen und Hilfsmittel benutzt zu haben.

Unterschrift: München, 4. Juli 2016.